Loss and Decoherence at the Quantum Hall-Superconductor Interface

Lingfei Zhao, Zubair Iftikhar, Trevyn F. Q. Larson, Ethan G. Arnault, Kenji Watanabe, Takashi Taniguchi, François Amet, and Gleb Finkelstein

Phys. Rev. Lett. **131**, 176604 — Published 27 October 2023

DOI: 10.1103/PhysRevLett.131.176604

Loss and decoherence at the quantum Hall - superconductor interface

Lingfei Zhao,[1,*] Zubair Iftikhar,[1] Trevyn F.Q. Larson,[1] Ethan G. Arnault,[1]
Kenji Watanabe,[2] Takashi Taniguchi,[2] François Amet,[3] and Gleb Finkelstein[1]

[1]*Department of Physics, Duke University, Durham, NC 27708, USA*
[2]*National Institute for Materials Science, 1-1 Namiki, Tsukuba 305-0044, Japan*
[3]*Department of Physics and Astronomy, Appalachian State University, Boone, NC 28607, USA*

(Dated: October 2, 2023)

We perform a systematic study of Andreev conversion at the interface between a superconductor and graphene in the quantum Hall (QH) regime. We find that the probability of Andreev conversion from electrons to holes follows an unexpected but clear trend: the dependencies on temperature and magnetic field are nearly decoupled. We discuss these trends and the role of the superconducting vortices, whose normal cores could both absorb and dephase the individual electrons in a QH edge. Our study may pave the road to engineering future generation of hybrid devices for exploiting superconductivity proximity in chiral channels.

Combining superconductors and quantum Hall (QH) systems has been proposed as a particularly promising direction for creating novel topological states and excitations [1]. Over the past few years, significant progress has been achieved in developing such hybrid structures [2–14]. In particular, hybridization of QH edge states across a narrow superconducting wire is expected to create a gapped topological superconductor [6, 15]. In the fractional QH systems, the strong interactions potentially fractionalize Majorana fermions into parafermions [13, 16], a key ingredient for universal topological quantum computing [1] and exotic circuit elements such as fractional charge transistors [15].

At the interface between a superconductor and a QH system, the QH edge states are expected to be proximitized, turning into chiral Andreev edge states (CAES). These are dispersive states which hybridize the electron and the hole amplitudes [17]. An electron approaching the superconducting region is converted to a linear combination of CAES, which interfere as they propagate along the interface. The outgoing particle can either stay as an electron or turn into a hole. We have previously observed clear evidence of the electron-hole conversion in the quantum Hall devices with superconducting contacts [12]. However, the exact mechanism of this conversion remains open: the role of the disorder, superconducting vortices, and the exact nature of the CAES in this system have been discussed. It is known that in order to observe a strong Andreev conversion in an ideal system a precise matching between the superconductor and the QH edge state momenta is required [18–21]. However, the presence of disorder is expected to relax this constraint [22, 23]. Vortices in the superconductor and extra QH channels induced by doping could also modify the signal [22–25]. In particular, the normal cores of the vortices can absorb the electrons and holes, reducing the amplitude of the measured signal [12, 23, 26].

To address the microscopic mechanisms affecting the Andreev conversion, here we perform a systematic study of the conversion probability vs temperature, T, magnetic field, B, and interfacial length, L. We find that the dependence of the electron-hole conversion probability on magnetic field and temperature nearly factorizes. We suggest a simple phenomenological expression involving exponential decays as a function of B, T and L, and a prefactor determined by the configuration of superconducting vortices. The expression captures the observed dependencies very well, and can be interpreted in terms of the CAES loss and decoherence. We finally discuss the distribution of the Andreev conversion probability [23], which is unexpectedly found to have a roughly triangular shape. We discuss the implications of our findings for the future development of the more complex devices, which will further explore the physics of superconducting correlations in the chiral states.

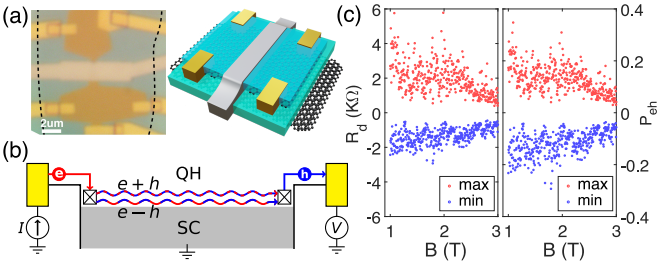

FIG. 1. (a) Optical image (left) and 3D schematics (right) of the device. The black dashed lines label the boundaries of the graphite gate underneath. The yellow electrodes are normal Cr/Au contacts and the light gray is the superconducting MoRe, which forms 0.5 μm and 1 μm interfaces with graphene. (b) Sketch of the measurement setup. The current is injected from the upstream contact into the grounded superconductor, while measuring the voltage at the downstream contact. (c) The maximum and minimum values of R_d (left) and P_{eh} (right) measured for the shorter interface. The statistical information is collected in the V_G range corresponding to $\nu = 2$, as outlined by the green lines in Fig. 3a. The temperature is 40 mK.

The main device studied here is a hBN/graphene/hBN heterostructure in contact with both superconducting and normal electrodes (Fig. 1a). The superconducting electrode (light gray) is made of sputtered Mo-Re alloy (50-50 in weight) with a critical temperature $T_c \sim 10$ K and an upper critical field H_{c2} exceeding 12 T. The work function of the alloy ~ 4.2 eV [27] is slightly lower than that of graphene ~ 4.5 eV [28], resulting in an n-doped graphene region nearby. The graphene sheet is separated into two independent regions by the etching

step that defines the superconducting electrode. The widths of the resulting superconductor-graphene interfaces are 0.5 and 1 μm. The normal contacts (yellow) are thermally evaporated Cr/Au. The electron density inside the graphene is controlled by applying a voltage V_G to the graphite gate which spans the whole area underneath the heterostructure. While such graphite gates are known to efficiently screen the disorder potential, the results here are similar to our previous measurements of samples without the graphite gate. This indicates that the observed physics is not strongly influenced by the disorder in the graphene layer.

We measure the nonlocal resistance downstream of a grounded superconducting contact, $R_d = dV_d/dI$, as sketched in Fig. 1b and demonstrated in the supplementary [29]. The CAES formed by the superconductor travel along the interface and recombine into either an electron or hole (or their linear combination) at the end of the interface. Sweeping the gate voltage V_G on top of the QH plateau tunes the momentum difference between the interfering CAES and produces an oscillating pattern of $R_d(V_G)$ (Fig. S1 in [29]) [12]. Due to the disordered nature of the interface, these interference patterns are highly irregular and resemble the universal conductance fluctuations [22, 23]. Throughout the paper we analyze the statistical properties of these patterns.

We further convert R_d into the difference between the probabilities of normal and Andreev reflections, $P_{eh} \equiv P_e - P_h$, where P_e (P_h) is the probability of an electron (or a hole) to be emitted downstream of the superconductor. It is straightforward to show that $P_{eh} = R_d/(R_d + R_H)$, where R_H is the Hall resistance [12]. Note that the extreme values of R_d are reached either for the pure electron reflection ($P_e = 1$, $P_h = 0$ and $R_d = \infty$, the interface is effectively fully opaque), or for perfect Andreev conversion ($P_e = 0$, $P_h = 1$, $R_d = -R_H/2$, a Cooper pair is transferred across the interface per incoming electron). We therefore expect that the distribution of R_d should be skewed toward positive resistances.

Indeed, this skewness can be observed by studying an imbalance between the maximum and minimum values of the downstream resistance $R_d(V_G)$. We extract these quantities in the V_G range corresponding to the $\nu = 2$ plateau for a given field and then plot R_{max} and R_{min} as a function of B in Fig. 1c. The field changes the vortex configuration every few mT [12], thereby allowing us to sample multiple different patterns of $R_d(V_G)$. The data clearly shows that R_{max} is on average larger than $|R_{min}|$. The apparent imbalance between electrons and holes is eliminated by converting R_d to P_{eh} in Fig. 1c. (See Fig. S3 in [29] for the similar result measured in another device.) We conclude that the probabilities of an electron or a hole being emitted downstream (P_e and P_h) are very similar. From now on, we present P_{eh} in lieu of R_d.

Depending on the length of the interface, the highest electron-hole conversion efficiency we observe is about 0.2 – 0.3. While being very high, this value is still far from reaching unity. Thermal smearing, decoherence and tunneling into the normal vortex cores can all contribute to this suppression. Since at zero temperature only the effect of the vortices remains, we first look into the dependence of P_{eh} on temperature. Fig. 2a plots P_{eh} of the shorter interface (0.5 μm) measured over the $\nu = 2$ plateau at $B = 2.2$ T from 40 mK to 670 mK. As the temperature T increases, P_{eh} gradually decays towards zero, except around 400 mK where the traces briefly jump to a completely different oscillation pattern. We attribute this jump to a temporary change of the configuration of superconducting vortices during the measurement.

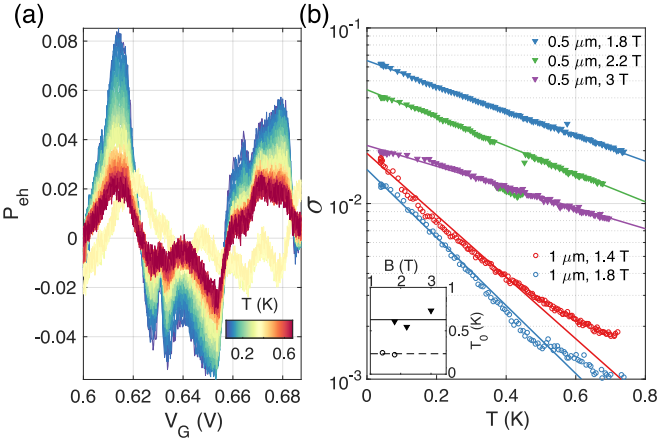

FIG. 2. (a) P_{eh} measured for the 0.5 μm interface as a function of V_G on top of the $\nu = 2$ plateau at $B = 2.2$ T. The temperature is varied from the base temperature of 40 mK to about 670 mK. (b) The standard deviation of P_{eh} of the 0.5 μm (filled triangle) and 1 μm (open circle) interfaces as a function of temperature at various magnetic fields. The inset plots the decay constant T_0 obtained from exponential fits vs. the magnetic field. The lines represent the averages of the dots.

To get a quantitative understanding of the thermal effects, we plot the standard deviation of the traces, σ, as a function of temperature in Fig. 2b for both interfaces at various magnetic fields. The filled triangles (open circles) represent $L = 0.5$ μm (1 μm). The green triangles correspond to the data in Fig. 2a. We find an exponential decay of σ as a function of temperature, i.e. $\sigma \propto \exp(-T/T_0)$, where T_0 is the decay constant. Remarkably, σ follows roughly the same decay rate for a given interface length. Even the curves of Fig. 2a which experienced a random jump follow the same slope. (Note the few green symbols nearly overlapping with the purple ones around 0.4 K.) This means that the configuration of superconducting vortices does not have a strong influence on the temperature dependence, even if it dramatically affects the amplitude and the pattern of fluctuations!

The exponential decay is observed regardless of the length of the interface and the magnetic field. For the longer interface, the decay rate becomes less steep at higher temperatures, but only as the signals approach the noise floor of a few $\times 10^{-3}$, so we extract the slope from the low-temperature range. In the inset of Fig. 2b, we plot the resulting T_0 vs. B for $L = 0.5$ and 1 μm. It is clear that T_0 does not show any strong dependence on B and scales inversely with L.

In principle, the exponential temperature dependence could

originate from the averaging over energy, like the thermal smearing of oscillations in a QH Fabry-Perot interferometer. However, the effects of thermal smearing are expected to saturate below T_0, while we observe an exponential decay down to temperatures more than 10 times lower (for the shorter interface). Moreover, thermal smearing is predicted to be rather inefficient in this system [23], because Andreev conversion is only weakly energy dependent. Furthermore, thermal broadening would smear the fluctuations of P_{eh} over V_G. Instead, we observe that the fluctuations in Fig. 2a uniformly decay with temperature with no noticeable smearing. In fact, we show that curves in Fig. 2a could be rescaled to nearly match (see Fig. S5 in [29]).

We therefore ascribe the temperature decay of P_{eh} to the decoherence of the CAES. Indeed, decoherence resulting in the exponential suppression of the oscillations $\propto \exp(-T/T_0)$ has been measured in Mach-Zehnder interferometers [30, 31]. However, the coherence length of the QH interferometers usually exceeds the length of the superconducting contact by more than an order of magnitude, including our own measurements using similar graphene samples [32]. The rapid decoherence of the CAES as compared to the QH edge states is likely due to their hybrid nature: The electron and the hole components should acquire an opposite phase in the fluctuating electrostatic potential. The source of these fluctuations could be the gate, or the vortex cores, which serve as a reservoir of normal electrons located next to the CAES.

Since T_0 is not strongly affected by the magnetic field and the jumps of the vortex configuration, the effects of the vortices should be primarily encoded in the zero temperature value of σ. The base temperature of 40 mK $\ll T_0$ allows us to use the corresponding values of σ as a close approximation to zero temperature value. In the following section, we study the dependence of this quantity on the magnetic field.

In Fig. 3a we show the patterns of P_{eh} over a wide range of magnetic field for the 0.5 μm interface (left) and the 1 μm interface (right). A corresponding Hall conductance map is shown in Fig. S2 [29]. The boundaries of the $\nu = 2$ plateau are labeled by the green lines. The amplitude of P_{eh} for the longer interface is not only smaller but also decays much faster with increasing B. This is consistent with our picture of electrons/holes tunneling from the edge state into the normal cores of the superconducting vortices. Indeed, the probability grows with both L and the vortex density, which increases with B.

While the dependence of P_{eh} on B is highly stochastic (Fig. 1c & S6 in [29]), we can analyze the large-scale trend by averaging σ over a relatively small range of magnetic fields, $\Delta B = 100$ mT. The resulting quantity averages over multiple vortex configurations and will be denoted by $\langle\sigma\rangle_{\Delta B}$. As shown in Fig. 3b, it roughly follows an exponential decay with B for both interfaces. Excluding the points that reach the noise floor, an exponential fit produces $B_0 = 1.84$ T for $L = 0.5$ μm and $B_0 = 0.85$ T for $L = 1$ μm, in agreement with the expected relation $B_0 \propto 1/L$.

Note that this relation further implies an exponential decay

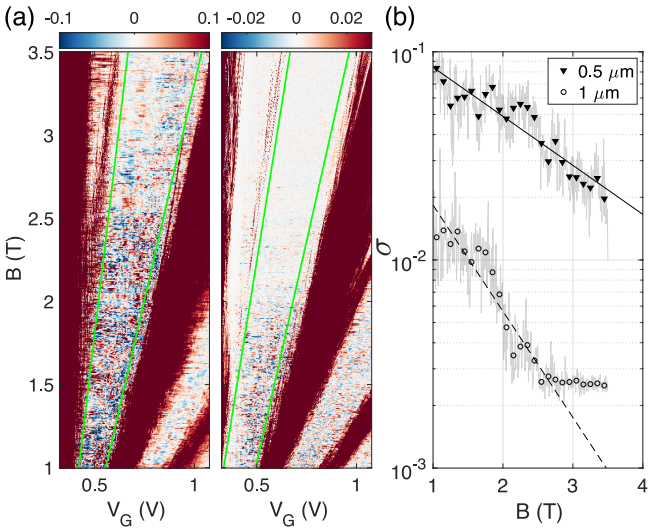

FIG. 3. (a) P_{eh} plotted against B and V_G for $L = 0.5$ μm (left) and 1 μm (right) at $T = 40$ mK. The green lines mark the region of the $\nu = 2$ plateau used for the analysis in panel (b) and Fig. 1c. (b) The standard deviation σ of P_{eh} measured over the V_G range corresponding to $\nu = 2$. The top and bottom gray curves correspond to the $L = 0.5$ and 1 μm interfaces. The lower curve saturates upon reaching the noise floor of the experiment, at $\sigma \approx 2.5 \times 10^{-3}$. The symbols (circles and triangles) represent σ averaged over 100 mT range, $\langle\sigma\rangle_{\Delta B}$. This averaging reveals the overall decay trend of σ, represented by the exponential fits (straight solid and dashed lines).

of $\langle\sigma\rangle_{\Delta B}$ as a function of L, $\langle\sigma\rangle_{\Delta B} \propto \exp\left(-L/L_0(B)\right)$ with $L_0 \propto 1/B$ at zero temperature. This dependence indicates that the electrons/holes are efficiently absorbed by multiple vortices, so that the inverse decay length $1/L_0$ is proportional to the vortex density $\propto B$ [23]. The $\exp\left(-L/L_0\right)$ dependence is directly confirmed in another device with three contacts of different interface length, as shown in Fig. S4 [29]. Interestingly, both devices have similar L_0 in the $250 - 300$ nm range at 1.5 T.

To summarize the observed trends, we can write

$$\sigma = A(\{\mathbf{r}_{vortex}\}) \exp\left(-\frac{B}{B_0(L)}\right) \times \exp\left(-\frac{T}{T_0(L)}\right) \quad (1)$$

where prefactor A represents fluctuations on the scale of a few mT due to vortex rearrangements. Importantly the decay rate B_0 is mostly independent of T, and T_0 is mostly independent of B (see Fig. 2b), which supports our assertion that different mechanisms are responsible for the B and T dependencies.

So far we have only considered the standard deviation of P_{eh}, but it is informative to further look into its full distribution. In Fig. 4a we plot the histogram of P_{eh} of the 1μm interface over a small range of $B = 1.4 - 1.5$ T. The range $\Delta B = 100$ mT is selected because on the one hand it covers many vortex rearrangements; on the other hand $\Delta B = 100$ mT $\ll B_0 = 0.85$ T so that the systematic reduction of the amplitude $\exp(-\Delta B/B_0)$ is negligible. The measured histogram is clearly peaked around zero, which contrasts with the uniform (rectangular) distribution predicted in Ref. [23].

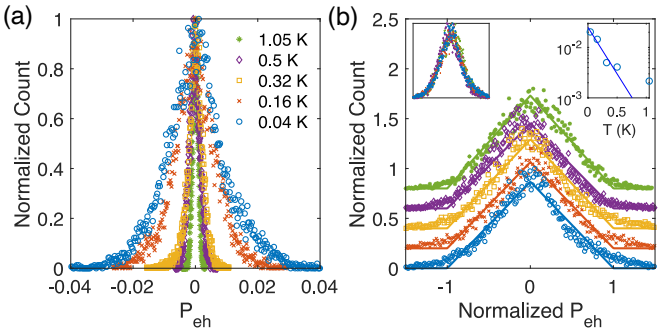

FIG. 4. (a) Histograms of P_{eh} collected for the longer interface in the $1.4-1.5$ T window on the $\nu=2$ plateau at various temperatures. (b) The same data as in (a) rescaled by fitting a phenomenological triangular shape (lines) and normalizing x-axis by the fitted width of the triangle. The curves are offset by 0.2 along the y-axis. Left inset: the same normalized distributions replotted without an offset. Right inset: the fitted width of the triangle plotted vs. T. The line is a guide for the eye, which follows the decay constant T_0 obtained in Fig. 2b.

While the distribution gets narrower with increasing temperature, the shape remains roughly the same, as seen in Fig. 4b, which replots the histograms with the x-axis normalized by their widths. These widths are plotted in the right inset of Fig. 4b (circles), together with an exponential line whose slope is determined by the constant T_0 obtained from Fig. 2b. The decay of the distribution widths with temperature agrees with the line, except for the highest temperature, which is likely limited by the noise in determining P_{eh}.

The distribution shape is expected to be influenced by the positions of the vortices, resulting in the random spread of $A\left(\{\mathbf{r}_{vortex}\}\right)$ (see Fig. 1c & S6 in [29]). To evaluate and eventually eliminate the variations of the P_{eh} due to vortex rearrangements, we normalize each $P_{eh}(V_G)$ trace by its standard deviation calculated for the same B. The resulting histograms of $P_{eh}(V_G)/\sigma$ are shown in Fig. S7 [29] and appear to have a roughly triangular shape similar to those in Fig. 4. We conclude that vortex rearrangements, while quite noticeable, cannot explain the shape of the P_{eh} distribution.

In principle, the non-rectangular distribution of P_{eh} may point to factors that have not yet been fully understood: spin-orbit coupling, interface transparency, contact doping, or specifics of graphene band structure. In particular, if the Andreev conversion probabilities for the two spins states are sufficiently different, the convolution of their rectangular distributions would produce a triangle. Regardless of these mechanisms, the distribution of the P_{eh} should be strongly shaped by the particle losses. In the supplementary [29], we present a toy model which qualitatively reproduces the observed distribution (Fig. S8). In the model, the CAES propagation along the interface is represented by the evolution of a 2×2 electron/hole density matrix, represented by a trajectory on the Bloch sphere [23]. The key insight of the model is that the losses have uneven effect on different trajectories: Most of the trajectories undergo heavy losses, resulting in a small P_{eh} that contributes to the center of the distribution peak. The rare trajectories which suffered less losses contribute to the tails of the distribution.

In summary, we have reported a systematic investigation of the Andreev conversion probability for the CAES states propagating along a superconducting contact in the QH regime. The main result is the near decoupling of the P_{eh} dependencies on the temperature and magnetic field, i.e. Eq. 1. The dependence on magnetic field, $A(\{\mathbf{r}_{vortex}\})\exp\left(-B/B_0\right)$ describes the particle loss, where the characteristic field B_0 decays with the interface length L in agreement with the theoretical prediction [23]. It is natural to associate the temperature dependence, $\exp\left(-T/T_0\right)$, with decoherence, which is found to be much more efficient compared to the conventional edge states in quantum Hall interferometers. Indeed, the relative phase of the electron and hole components of the CAES should be strongly influenced by the fluctuations of electric environment. Understanding and controling the loss and decoherence processes is crucial for the development of future devices that utilize superconducting correlations in chiral states.

We greatly appreciate stimulating discussion with A. Akhmerov, H. Baranger, L. Glazman, V. Kurilovich, A. Manesco, Y. Oreg, E. Sela, and A. Stern. Sample fabrication and characterization by L.Z. and E.A. were supported by NSF award DMR-2004870. Transport measurements by L.Z. and T.L. and data analysis by L.Z., Z.I. and G.F. were supported by the Division of Materials Sciences and Engineering, Office of Basic Energy Sciences, U.S. Department of Energy, under Award No. DE-SC0002765. The deposition of MoRe performed by F.A. was supported by a URC grant at Appalachian State University. K.W. and T.T. acknowledge support from the Elemental Strategy Initiative conducted by the MEXT, Japan, (grant no. JPMXP0112101001), JSPS KAKENHI (grant no. JP20H00354) and CREST (no. JPMJCR15F3, JST). The sample fabrication was performed in part at the Duke University Shared Materials Instrumentation Facility (SMIF), a member of the North Carolina Research Triangle Nanotechnology Network (RTNN), which is supported by the National Science Foundation (Grant ECCS-1542015) as part of the National Nanotechnology Coordinated Infrastructure (NNCI).

* lz117@duke.edu

[1] R. S. K. Mong, D. J. Clarke, J. Alicea, N. H. Lindner, P. Fendley, C. Nayak, Y. Oreg, A. Stern, E. Berg, K. Shtengel, and M. P. A. Fisher, Phys. Rev. X **4**, 011036 (2014).
[2] P. Rickhaus, M. Weiss, L. Marot, and C. Schönenberger, Nano Letters **12**, 1942 (2012).
[3] K. Komatsu, C. Li, S. Autier-Laurent, H. Bouchiat, and S. Guéron, Phys. Rev. B **86**, 115412 (2012).
[4] Z. Wan, A. Kazakov, M. J. Manfra, L. N. Pfeiffer, K. W. West, and L. P. Rokhinson, Nature Communications **6**, 7462 (2015).
[5] F. Amet, C. T. Ke, I. V. Borzenets, J. Wang, K. Watanabe, T. Taniguchi, R. S. Deacon, M. Yamamoto, Y. Bomze, S. Tarucha, and G. Finkelstein, Science **352**, 966 (2016).
[6] G.-H. Lee, K.-F. Huang, D. K. Efetov, D. S. Wei, S. Hart, T. Taniguchi, K. Watanabe, A. Yacoby, and P. Kim, Nature

Physics **13**, 693 (2017).
[7] G.-H. Park, M. Kim, K. Watanabe, T. Taniguchi, and H.-J. Lee, Scientific Reports **7**, 10953 (2017).
[8] M. R. Sahu, X. Liu, A. K. Paul, S. Das, P. Raychaudhuri, J. K. Jain, and A. Das, Phys. Rev. Lett. **121**, 086809 (2018).
[9] S. Matsuo, K. Ueda, S. Baba, H. Kamata, M. Tateno, J. Shabani, C. J. Palmstrøm, and S. Tarucha, Scientific Reports **8**, 3454 (2018).
[10] Y. Kozuka, A. Sakaguchi, J. Falson, A. Tsukazaki, and M. Kawasaki, Journal of the Physical Society of Japan **87**, 124712 (2018).
[11] A. Seredinski, A. W. Draelos, E. G. Arnault, M.-T. Wei, H. Li, T. Fleming, K. Watanabe, T. Taniguchi, F. Amet, and G. Finkelstein, Science Advances **5**, eaaw8693 (2019).
[12] L. Zhao, E. G. Arnault, A. Bondarev, A. Seredinski, T. F. Q. Larson, A. W. Draelos, H. Li, K. Watanabe, T. Taniguchi, F. Amet, H. U. Baranger, and G. Finkelstein, Nature Physics **16**, 862 (2020).
[13] O. Gül, Y. Ronen, S. Y. Lee, H. Shapourian, J. Zauberman, Y. H. Lee, K. Watanabe, T. Taniguchi, A. Vishwanath, A. Yacoby, and P. Kim, Phys. Rev. X **12**, 021057 (2022).
[14] M. Hatefipour, J. J. Cuozzo, J. Kanter, W. M. Strickland, C. R. Allemang, T.-M. Lu, E. Rossi, and J. Shabani, Nano Letters **22**, 6173 (2022).
[15] D. J. Clarke, J. Alicea, and K. Shtengel, Nature Physics **10**, 877 (2014).
[16] D. J. Clarke, J. Alicea, and K. Shtengel, Nature Communications **4**, 1348 (2013).
[17] H. Hoppe, U. Zülicke, and G. Schön, Physical Review Letters **84**, 1804 (2000).
[18] F. Giazotto, M. Governale, U. Zülicke, and F. Beltram, Phys. Rev. B **72**, 054518 (2005).
[19] A. R. Akhmerov and C. W. J. Beenakker, Phys. Rev. Lett. **98**, 157003 (2007).
[20] J. A. M. van Ostaay, A. R. Akhmerov, and C. W. J. Beenakker, Phys. Rev. B **83**, 195441 (2011).
[21] A. B. Michelsen, P. Recher, B. Braunecker, and T. L. Schmidt, Phys. Rev. Res. **5**, 013066 (2023).
[22] A. L. R. Manesco, I. M. Flór, C.-X. Liu, and A. R. Akhmerov, SciPost Phys. Core **5**, 045 (2022).
[23] V. D. Kurilovich, Z. M. Raines, and L. I. Glazman, Nature Communications **14**, 2237 (2023).
[24] Y. Tang, C. Knapp, and J. Alicea, Phys. Rev. B **106**, 245411 (2022).
[25] A. David, J. S. Meyer, and M. Houzet, Phys. Rev. B **107**, 125416 (2023).
[26] N. Schiller, B. A. Katzir, A. Stern, E. Berg, N. H. Lindner, and Y. Oreg, Phys. Rev. B **107**, L161105 (2023).
[27] S. Hałas, T. Pieńkos, M. Czarnacki, and T. Durakiewicz, Vacuum **82**, 1094 (2008).
[28] S.-J. Liang and L. K. Ang, Phys. Rev. Appl. **3**, 014002 (2015).
[29] See Supplemental Material (which includes Ref. [33]) at [URL will be inserted by publisher] for the additional figures and notes on 1) the device fabrication and measurement methods, 2) the comparison to the data of a non-superconducting interface, 3) the data measured in additional samples, 4) the uniform temperature dependence of $P_{eh}(V_G)$, 5) the variation of signal due to rearrangement of vortices, 6) the histograms of normalized σ and 7) the toy model for the distribution of P_{eh}.
[30] Y. Ji, Y. Chung, D. Sprinzak, M. Heiblum, D. Mahalu, and H. Shtrikman, Nature **422**, 415 (2003).
[31] P. Roulleau, F. Portier, P. Roche, A. Cavanna, G. Faini, U. Gennser, and D. Mailly, Phys. Rev. Lett. **100**, 126802 (2008).
[32] L. Zhao, E. G. Arnault, T. F. Q. Larson, Z. Iftikhar, A. Seredinski, T. Fleming, K. Watanabe, T. Taniguchi, F. Amet, and G. Finkelstein, Nano Letters **22**, 9645 (2022).
[33] C. Caroli, P. D. Gennes, and J. Matricon, Physics Letters **9**, 307 (1964).